Case Studies in Thermal Engineering 28 (2021) 101355

Contents lists available at ScienceDirect

Case Studies in Thermal Engineering

journal homepage: www.elsevier.com/locate/csite

Free vibrations of rotating CNTRC beams in thermal environment

Xinli Xu [a], Chunwei Zhang [a,*], Afrasyab Khan [b], Tamer A. Sebaey [c,d], Mohammad Alkhedher [e]

[a] Structural Vibration Control Group, Qingdao University of Technology, Qingdao, 266033, China
[b] Institute of Engineering and Technology, Department of Hydraulics and Hydraulic and Pneumatic Systems, South Ural State University, Lenin Prospect 76, Chelyabinsk, 454080, Russian Federation
[c] Engineering Management Department, College of Engineering, Prince Sultan University, Riyadh, Saudi Arabia
[d] Mechanical Design and Production Department, Faculty of Engineering, Zagazig University, P.O. Box 44519, Zagazig, Sharkia, Egypt
[e] Mechanical Engineering Department, Abu Dhabi University, United Arab Emirates

ARTICLE INFO

Keywords:
Free vibrations
Post-buckled natural frequency
Rotating nanocomposite beams
Carbon nanotube
Boundary condition type

ABSTRACT

A study on the first natural frequency of rotating nanocomposite beams is addressed in this research. The beam has been reinforced with carbon nanotube. With the purpose of incorporating the shearability of the beam, the Reddy's third order shear deformation theory has been assigned. The motion equations are discretized in space employing the well-know Ritz-technique. For the sake of study on the first natural frequency, the nonlinear in time discretized equations of motion are linearized around the static deformation induced by the centrifugal force. The linearized discretized governing equations around the post-buckling state are exploited to find the first natural frequency after the buckling incidence. The outcomes reveal that although a stationary free-clamped(simply-clamped) beam and a stationary clamped-free(clamped-simply) beam treat similarly in the analyses, the associated rotating beams demonstrate a qualitative discrepancy. Moreover, the outcomes based upon the Reddy's third order shear deformation theory deviate from the results in regard of the Timoshenko beam theory approximately below the length to the height of the beam equal to 12 for CS FGX CNTRC beams. Nevertheless, for the FGO CNTRC beams the results in reference to the both mentioned theories approximately are consistent to each other.

1. Introduction

In various industries from a rotating wheel space station to a micro turbine in cell phones, rotating systems are a widely implemented part. The common part in rotating systems is a rotating beam which it may be a simplified model for a blade. Moreover, because of the outstanding thermo-mechanical characteristics of two-phase nanocomposite materials, appointing the substance of rotating beams from the nanocomposite materials may empower efficiently the mechanical behavior of the rotating beams. Furthermore, during the life cycle of a rotating beam, it may encounter difficult spots such as temperature rising. Moreover, different applications may require different boundary condition types. Accordingly, this research looks forward to examine comprehensively the fundamental natural frequency of rotating nanocomposite beams reinforced with carbon nano tube (CNT) (CNTRC beams) when they deal with different loading situations. In the best knowledge of the authors the free vibrations of rotating CNTRC beams prior to and

* Corresponding author.
E-mail address: zhangchunwei@qut.edu.cn (C. Zhang).

https://doi.org/10.1016/j.csite.2021.101355
Received 19 June 2021; Received in revised form 10 August 2021; Accepted 15 August 2021
Available online 4 September 2021

after experiencing the instability owing to the buckling incidence have not been studied yet. Moreover, the developed dynamics formulation for the rotating CNTRC beams in the context of the third-order shear deformation theory proposed by Reddy (RSDT) (Ref. [1]) is also another originality of the current paper. Furthermore, the applicability of the Timoshenko beam theory is also discussed in details in terms of CNT distribution pattern type and the boundary condition type. The followings clarify the aforementioned innovations of the present research.

The natural frequencies and buckling instability analyses of stationary functionally graded (FG)/CNTRC beams prior to and after the buckling occurrence were examined in various works. Zhu et al. [2] studied on the static response and free vibration features of CNTRC plates. A multiscale technique was developed by Shen and Xiang [3] to study on the nonlinear natural frequencies and the post-buckling amplitude of CNTRC beams. They announced that increasing the CNT volume fraction does not necessarily enlarge the nonlinear natural frequency. Lin and Xiang [4] investigated on the natural frequencies of CNTRC beams in the framework of Timoshenko beam theory and RSDT. The influence of the applied shear deformation theory on the outcomes was investigated. Selim et al. [5] established an examination to analyze the free vibrations of FG plates subjected to a thermal ambient in the framework of RSDT. Safaei et al. [6] developed a precise molecular mechanics model for buckling instability analysis of multi-walled carbon nanotubes MWCNT subjected to a mechanical compression. Mirjavadi et al. [7] studied on the thermal buckling instability of imperfect FG porous microbeams. The size dependency was incorporated to the developed formulation employing the MCST hypotheses. Sahmani and Aghdam [8] explored the buckling instability and the post-critical deflection of nanoplates reinforced with graphene platelet (GPL) subjected to compressive mechanical loads in the framework of the nonlocal strain gradient theory (SGT). The Euler-Bernoulli beam assumptions were used to explore the buckling and free vibrations of FG nanobeams by Mirjavadi et al. [9]. To encompass the size dependency to the governing equations the Eringen's nonlocal elasticity theory was employed. Shen et al. [10] examined the buckling instability and post-critical deflection of GPL plates subjected to a temperature increment. A study on the buckling instability and free vibrations of porous GPL nanocomposite plates was established by Yang et al. [11]. Mirjavadi et al. [12] investigated on the natural frequencies of FG micro beams in thermal ambient considering the porosity influence. The equations of motion were obtained in reliance on the Timoshenko beam theory alongside the modified couple stress theory (MCST). Lin et al. [13] addressed the dynamic and static instability of GPL nanocomposite plates with piezoelectric layers. Hamzah et al. [14] established an analysis to examine the free vibrations of cylindrical shells undergone a temperature change. The buckling and crushing treatment of foam core composite sandwich columns subjected to an edgewise compressive force were examined by Eyvaziyan et al. [15]. To increases the critical load a particular fixture was devised to fasten transversely the sandwich column. An investigation on the buckling instability and post-critical deflection of GPL piezoelectric plates undergone an electric potential and compressive forces was executed by Mao and Zhang [16]. Fattahi et al. [17] investigated on the size-dependent buckling instability of single-layered graphene sheets embedded in an elastic foundation. Eyvazian et al. [18] established an investigation to examine the free vibrations of viscoelastic smart sandwich GPL plates with magnetorheological fluid core bonded with piezo-magnetic facesheets. Zhao et al. [19] investigated on the free vibrations of FG CNTRC truncated canonical conical panels. An examination on the influence of porosity of the core layer on the vibrational treatment of multilayered composite plates was established by Safaei [20]. Eyvazian et al. [21] investigated on the dynamics of GPL nano cylindrical shells undergone a moving harmonic excitation employing the nonlocal SGT. The impacts of the GPL weight fraction and the size dependency on the outcomes were analyzed. Zhao et al. [22] proposed an analytical solution for the sake of the examination of the forced vibrations of micro-/nanobeams in thermal ambient by the implementation of Green's functions. Zheng et al. [23] studied on the thermo-mechanical buckling of GPL sandwich piezoelectric microplates. The impression of the dispersion type on the outcomes highlighted the significance of the distribution pattern kind. The free vibrations of FG plates subjected to temperature change was examined by Tran et al. [24]. Li et al. [25] examined the static displacement of FG structures subjected to a thermo-mechanical load. Fattahi et al. [26] addressed an experimental examination to illuminate the variation of elastic features of high density polyethylene-MWCNT nanocomposites with respect to the nanoparticle volume fraction.

The vibrations of rotating beams were also discussed widely in numerous papers. Arvin [27] used the direct method of multiple scales (MMS) to explore the principal parametric resonance of rotating isotropic clamped-free (CF) beams. The frequency of the variable term of the rotation speed was considered to be two times a natural frequency. The damping coefficient efficacy on the critical parametric excitation amplitude and the instability region was investigated. Heidari and Arvin [28] employed the direct MMS to examine the backbone curve of rotating CF CNTRC beams against the backdrop of the Timoshenko beam theory. The results illustrated that at the same condition, the CNT distribution pattern type can change the type of the nonlinearity of natural frequencies of rotating CNTRC beams.

Recently, the free vibrations of rotating beams prior to and after the buckling incidence were taken into consideration. The Timoshenko beam theory was implemented by Khosravi et al. [29] to analyze the natural frequencies as well as the corresponding mode shapes of rotating CNTRC beams in thermal ambient prior to the buckling incidence. The influences of boundary condition type and the CNT dispersion pattern type on the natural frequencies were illustrated. Hosseini and Arvin [30] studied on the first natural frequency of rotating sandwich FG Euler-Bernoulli microbeams prior to and after the buckling incidence. The MCST was employed to incorporate the size dependency to the governing equations. The impacts of the rotating speed and the geometrical features on the first natural frequency prior to and after the buckling occurrence were examined. Arvin et al. [31] applied the finite element technique to examine the first natural frequency of rotating FG beams in thermal ambient. The governing equations were developed in the reliance on the Euler-Bernoulli beam assumptions. Considering the dependence of the constituent of the FG material (FGM) on the temperature, the efficacy of the boundary condition as well as the FGM power law exponent on the free vibrations prior to and after the buckling occurrence was studied.

Thereupon, in the context of the RSDT, this research deals with the first natural frequency of rotating CNTRC beams subjected to a temperature increment prior to and after the buckling incidence. The increment of the temperature and the centrifugal force can

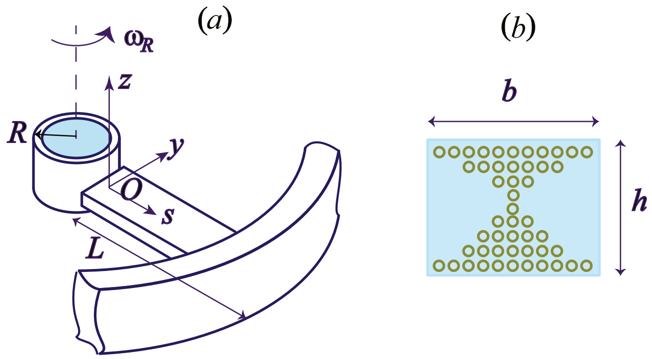

Fig. 1. (*a*) A a rotating FC CNTRC beam, (*b*) The FGO dispersion pattern.

Table 1
The CNT volume fraction for various CNT distribution patterns (Ref. [33]).

CNT distribution pattern	V_{CN}
UD	V_{CN}^{*}
FGX	$4V_{CN}^{*}\frac{\lvert z\rvert}{h}$
FGO	$2V_{CN}^{*}\left[1-2\frac{\lvert z\rvert}{h}\right]$

induce a mutual instability to rotating beams. With the purpose of discretizing the nonlinear motion equations in space the Ritz method is employed. Efficient algorithms are established to determine the post-buckling configuration. The fundamental natural frequency of the rotating CNTRC beam after the buckling incidence is defined by the implementation of the linearized equations around the post-buckling configuration. The CNT dispersion pattern, rotational speed, the support condition, the hub radius, and the length to the height of the beam impacts on the first natural frequency are demonstrated.

2. Eliciting motion equations

A rotating free-clamped (FC) FGO CNTRC beam is shown in Fig. 1. The origin of the rotating coordinate system, i.e. $O-(s,y,z)$, is placed at the center of the cross section bonded at the outer surface of the hub. The hub radius is R. The hub rotates with a steady speed ω_R. The axes of s, z, and y are directed toward the beam span, the beam height, and the beam width, in order. The beam geometrical characteristics, are, the beam length, L, the beam height, h, and the beam width, b, respectively.

2.1. The equivalence thermo-mechanical properties of a CNTRC beam

With the purpose of determination of the equivalent thermo-mechanical attributes of the CNTRC beam the refined rule of mixture developed by Ref. [32] is implemented. Accordingly, the Young moduli, i.e. E_{11}, and E_{22}, and the shear modulus, i.e. G_{12}, of an isotropic matrix reinforced with CNT are defined, respectively, by (Ref. [33]):

$$E_{11}=\eta_1 V_{CN}E_{11}^{CN}+V_mE^m,\quad \frac{\eta_2}{E_{22}}=\frac{V_{CN}}{E_{22}^{CN}}+\frac{V_m}{E^m},\quad \frac{\eta_3}{G_{12}}=\frac{V_{CN}}{G_{12}^{CN}}+\frac{V_m}{G^m}, \tag{1}$$

where hereafter, the scripts CN, and m are, respectively, stand for a feature referring to the CNT and the matrix phases. Moreover, eta_i's are the efficiency coefficients which are specified according to the total CNT volume fraction in a cross-section, i.e. V_{CN}^{*}. For the assumed total volume fraction in this paper which is $V_{CN}^{*}=0.17$, they are, $\eta_1=0.142$, $\eta_2=1.626$, and $\eta_3=0.7\eta_2$ (Ref. [33]). Furthermore, V_{CN} is the distribution function of the volume fraction of the CNT. It is presumed that the volume fraction of the CNT is invariant along the beam span and the beam width while it can be varied onward the height of the beam. The CNT volume fraction for three different dispersion pattern types is exposed in Table 1 (Ref. [33]):

It is worth to note that the CNT and the matrix volume fractions are relevant to each other via $V_{CN}+V_m=1$.

The Poisson's coefficient, i.e. ν_{12}, the mass density, i.e. ρ, and the thermal expansion constant, i.e. α_{11}, of the CNTRC beam are determined, in order, by (Ref. [33]):

$$\nu_{12} = V_{CN}^{*}\nu_{12}^{CN} + V_m\nu^m, \quad \frac{\nu_{21}}{E_{22}} = \frac{\nu_{12}}{E_{11}}, \\ \rho = V_{CN}\rho^{CN} + V_m\rho^m, \tag{2}$$

and

$$\alpha_{11} = \frac{V_{CN}E_{11}^{CN}\alpha_{11}^{CN} + V_mE^m\alpha^m}{V_{CN}E_{11}^{CN} + V_mE^m} \tag{3}$$

2.2. Mechanics of the rotating CNTRC beam

The RSDT (Ref. [1]) is employed to regard the shearability of the CNTRC beam. Subsequently, the axial displacement, i.e. u, and the deflection, i.e. w, for a material particle located at $P(s, y, z)$, at time t, read (Ref. [1]):

$$\begin{aligned} u(s,t) &= u_0(s,t) + z\psi(s,t) - az^3[\psi(s,t) + \partial_s w_0(s,t)] \\ w(s,t) &= w_0(s,t) \end{aligned} \tag{4}$$

wherein $a = 4/(3\,h^2)$, and ∂_s denotes the derivative in reference to s-variable of the forthcoming variable. Moreover, $u_0(s, t)$, and $w_0(s, t)$, are the axial displacement and the deflection of a material particle located at the mid-plane of the cross section of the early introduced material particle. Furthermore, $\psi(s, t)$ is the bending rotation of the cross section of the assumed material particle.

The nonlinear von-Karman relationships is admissible with the presumption of the moderate rotations and small strains (Ref. [1]). In this respect, the only non-zeros normal strain, i.e. ϵ_{ss}, and shear strain, i.e. γ_{sz}, read (Ref. [1]):

$$\epsilon_{ss} = \partial_s u + \frac{1}{2}[\partial_s w]^2, \tag{5}$$

and

$$\gamma_{sz} = \partial_z u + \partial_s w \tag{6}$$

The substitution of Eq. (4) into Eqs. (5), and (6), sequently, results in:

$$\epsilon_{ss} = \epsilon^{(0)}(s,t) + z\kappa(s,t) + z^3\epsilon^{(3)}(s,t) \tag{7}$$

and

$$\gamma_{sz} = \gamma_{sz}^{(0)} + z^2\gamma_{sz}^{(2)} \tag{8}$$

where

$$\epsilon^{(0)} = \partial_s u_0(s,t) + \frac{1}{2}\partial_s w_0(s,t)^2, \tag{9}$$

$$\kappa = \partial_s\psi(s,t), \tag{10}$$

$$\epsilon^{(3)} = -a\partial_s\psi(s,t) + \partial_{ss}w_0(s,t), \tag{11}$$

and

$$\gamma_{sz}^{(0)} = \psi(s,t) + \partial_s w_0(s,t), \tag{12}$$

and

$$\gamma_{sz}^{(2)} = -3a[\psi(s,t) + \partial_s w_0(s,t)] \tag{13}$$

A persistent temperature change, i.e. ΔT, is presumed along the height of the CNTRC beam. Thereupon, the normal stress, i.e. σ_{ss}, and the shear stress, i.e. τ_{sz}, relations in terms of the corresponding strains for a one-dimensional composite medium in thermal environment are implemented (Ref. [1]):

$$\sigma_{ss} = Q_{11}(z)[\epsilon_{ss} - \alpha_{11}(z)\Delta T], \tag{14}$$

and

$$\tau_{sz} = Q_{55}\gamma_{sz} \tag{15}$$

where $Q_{11}(z) = E_{11}/(1 - \nu_{12}\nu_{21})$, and $Q_{55} = G_{13}$ are the reduced plane-stress elastic stiffnesses.

2.3. Weak form of the motion equations

In view of the pertinence of the Ritz technique, this scheme is appointed with the aim of discretizing the motion equations in space. Since the Ritz scheme deals with the weak form of the motion equations (Ref. [34]), hence, the virtual strain and kinetic energies should be determined. The virtual strain energy, i.e. δU, for a one dimensional medium read (Ref. [35]):

$$\begin{aligned}\delta U &= \int_0^L \int_{-\frac{1}{2}h}^{\frac{1}{2}h} [\sigma_{ss}\delta\epsilon_{ss}(s,t) + \tau_{sz}\delta\gamma_{sz}]\mathrm{d}z\mathrm{d}s \\ &\int_0^L \int_{-\frac{1}{2}h}^{\frac{1}{2}h} [\sigma_{ss}\{\delta\epsilon^{(0)}(s,t) + z\delta\kappa(s,t) + z^3\delta\epsilon^{(3)}(s,t)\} + \tau_{sz}\{\delta\gamma_{sz}^{(0)} + z^2\delta\gamma_{sz}^{(2)}\}]\mathrm{d}z\mathrm{d}s\end{aligned} \tag{16}$$

The substitution of the stresses from Eqs. (14), and (15) into Eq. (16) releases the strain energy,

$$\delta U = \int_0^L [N_{ss}\delta\epsilon^{(0)}(s,t) + M_{ss}\delta\kappa(s,t) + R_{ss}\delta\epsilon^{(3)}(s,t) + Q_{sz}\delta\gamma_{sz}^{(0)} + P_{sz}\delta\gamma_{sz}^{(2)}]\mathrm{d}s \tag{17}$$

where N_{ss}, Q_{sz}, M_{ss}, R_{ss}, and P_{sz}, are, respectively, the stress and third-order stress resultants because of the implementation of the RSDT, expressed by:

$$N_{ss} = -N_{ss}^T + A_{11}\epsilon^{(0)}(s,t) + B_{11}\kappa(s,t) + C_{11}\epsilon^{(3)}(s,t), \tag{18}$$

$$Q_{sz} = A_{55}\gamma_{sz}^{(0)}(s,t) + D_{55}\gamma_{sz}^{(2)}(s,t), \tag{19}$$

$$M_{ss} = -M_{ss}^T + B_{11}\epsilon^{(0)}(s,t) + D_{11}\kappa(s,t) + F_{11}\epsilon^{(3)}(s,t), \tag{20}$$

$$R_{ss} = -R_{ss}^T + C_{11}\epsilon^{(0)}(s,t) + F_{11}\kappa(s,t) + G_{11}\epsilon^{(3)}(s,t), \tag{21}$$

and

$$P_{sz} = D_{55}\gamma_{sz}^{(0)}(s,t) + F_{55}\gamma_{sz}^{(2)}(s,t) \tag{22}$$

where N_{ss}^T, M_{ss}^T, and R_{ss}^T, are the thermal stress and higher order thermal stress resultants reported in Appendix. A_{ii}'s, B_{11}, C_{11}, D_{ii}'s, F_{ii}'s, and G_{11} are the CNTRC beam elastic stiffnesses defined in Appendix.

By substituting the required relations into Eq. (16), the virtual strain energy turns into:

$$\begin{aligned}\delta U &= \int_0^L \Bigg[\Bigg\{ -N_{ss}^T + A_{11}\left\{\partial_s u_0(s,t) + \frac{1}{2}\partial_s w_0(s,t)^2\right\} + B_{11}\{\partial_s\psi(s,t)\} + C_{11}\{-a\partial_s\psi(s,t) \\ &+ \partial_{ss}w_0(s,t)\}\Bigg\}\delta\left\{\partial_s u_0(s,t) + \frac{1}{2}\partial_s w_0(s,t)^2\right\} + \Bigg\{ -M_{ss}^T + B_{11}\left\{\partial_s u_0(s,t) + \frac{1}{2}\partial_s w_0(s,t)^2\right\} \\ &+ D_{11}\{\partial_s\psi(s,t)\} + F_{11}\{-a\partial_s\psi(s,t) + \partial_{ss}w_0(s,t)\}\Bigg\}\delta\{\partial_s\psi(s,t)\} + \Bigg\{ -R_{ss}^T + C_{11}\Big\{\partial_s u_0(s,t) \\ &+ \frac{1}{2}\partial_s w_0(s,t)^2\Big\} + F_{11}\{\partial_s\psi(s,t)\} + G_{11}\{-a\partial_s\psi(s,t) + \partial_{ss}w_0(s,t)\}\Bigg\} \\ &\delta\{-a\partial_s\psi(s,t) + \partial_{ss}w_0(s,t)\} \\ &+ \{A_{55}\{\psi(s,t) + \partial_s w_0(s,t)\} + D_{55}\{-3a[\psi(s,t) + \partial_s w_0(s,t)]\}\}\delta\{\psi(s,t) + \partial_s w_0(s,t)\} \\ &+ \{D_{55}\{\psi(s,t) + \partial_s w_0(s,t)\} + F_{55}\{-3a[\psi(s,t) + \partial_s w_0(s,t)]\}\}\delta\{-3a\psi(s,t) \\ &+ \partial_s w_0(s,t)]\}\Bigg]\mathrm{d}s\end{aligned} \tag{23}$$

The dynamical kinetic energy of a rotating one dimensional medium is determined by (Ref. [30]):

$$K = \frac{1}{2}\int_0^L \int_{-\frac{1}{2}h}^{\frac{1}{2}h} \rho(z)[(\partial_t u)^2 + (\partial_t w)^2]\mathrm{d}z\mathrm{d}s + \frac{1}{2}\int_0^L \int_{-\frac{1}{2}h}^{\frac{1}{2}h} \rho(z)[\omega_R^2(R + s + u)^2]\mathrm{d}z\mathrm{d}s \tag{24}$$

The replacement of the axial and transverse displacements from Eq. (4), reshuffles the kinetic energy relation, i.e. Eq. (24), into:

$$
\begin{aligned}
K = & \int_0^L \left\{ \frac{1}{2}a^2 I_6[\partial_t\psi(s,t) + \partial_{st}w_0(s,t)]^2 - aI_4\partial_t\psi(s,t)[\partial_t\psi(s,t) + \partial_{st}w_0(s,t)] \right. \\
& -aI_3\partial_t u_0(s,t)[\partial_t\psi(s,t) + \partial_{st}w_0(s,t)] \\
& +\frac{1}{2}I_2[\partial_t\psi(s,t)]^2 + I_1\partial_t u_0(s,t)\partial_t\psi(s,t) + \frac{1}{2}I_0[\partial_t u_0(s,t)]^2 + \frac{1}{2}I_0[\partial_t w_0(s,t)]^2 \\
& +\frac{1}{2}a^2 I_6\omega_R^2[\psi(s,t) + \partial_s w_0(s,t)]^2 - aI_4\omega_R^2\psi(s,t)[\psi(s,t) + \partial_s w_0(s,t)] \\
& -aI_3\omega_R^2[\psi(s,t) + \partial_s w_0(s,t)][R + s + u_0(s,t)] \\
& \left. +\frac{1}{2}I_2\omega_R^2\psi(s,t)^2 + I_1\omega_R^2\psi(s,t)[R + s + u_0(s,t)] + \frac{1}{2}I_0\omega_R^2[R + s + u_0(s,t)]^2 \right\} \mathrm{d}s
\end{aligned}
\tag{25}
$$

where I_i's are the inertial terms defined in Appendix.

Resorting to minimization of the action integral, i.e. S, (Ref. [35]), i.e. $\delta S = \int_{t_1}^{t_2}(\delta K - \delta U)\mathrm{d}t = 0$, the weak form of the motion equations is achieved.

2.4. The Ritz technique procedure exertion

For the sake of discretizing the weak form of the nonlinear motion equations in space the Ritz technique is utilized. Subsequently, the following relations for the displacement variables are considered to separate the equations of motion in time and space (Ref. [35]):

$$
\begin{aligned}
w_0(s,t) &= \Sigma_{i=0}^N[A_i(t)\phi_i^{(w)}(s)] \\
\psi(s,t) &= \Sigma_{m=0}^N[B_m(t)\phi_m^{(\psi)}(s)] \\
u_0(s,t) &= \Sigma_{r=0}^N[C_r(t)\phi_r^{(u)}(s)]
\end{aligned}
\tag{26}
$$

where N is the number of Ritz terms which are required in the convergence study, and $A_i(t)$, $B_m(t)$, and $C_r(t)$ are the Ritz coefficients which must be defined during the solution process. Moreover, $\phi_i^{(w)}(s)$, $\phi_m^{(\psi)}(s)$, and $\phi_r^{(u)}(s)$ are the associated assumed functions which must be selected to be an independent set while they satisfy the essential boundary conditions (Ref. [34]). In this respect, they can be chosen as a multiplication of two functions, i.e. $\phi_i^{(w)}(s) = R^w(s)T_i(s)$, $\phi_m^{(\psi)}(s) = R^\psi(s)T_i(s)$, and $\phi_r^{(u)}(s) = R^u(s)T_i(s)$; one satisfies the essential boundary conditions, i.e. $R^w(s)$, $R^\psi(s)$, and $R^u(s)$, and the other, i.e. $T_i(s)$ enforces the orthogonality condition to create an independent set.

With the aim of satisfying the essential boundary conditions the following polynomial form weight functions are considered (Ref. [36])

$$
R^w(s) = \left(\frac{s}{L}\right)^\alpha\left(1 - \frac{s}{L}\right)^\beta, \quad R^\psi(s) = \left(\frac{s}{L}\right)^\gamma\left(1 - \frac{s}{L}\right)^\delta, \quad R^u(s) = \left(\frac{s}{L}\right)^\xi\left(1 - \frac{s}{L}\right)^\varsigma
$$

in which for a specified boundary condition at the supports of the CNTRC beam the corresponding exponents for each displacement component can be 0, and 1, independently. If the RSDT is implemented, the exponent for the deflection can take the value 2. For instance, for a rotating FC CNTRC beam the weight functions are:

$$
R^w(s) = \left(\frac{s}{L}\right)^0\left(1 - \frac{s}{L}\right)^2, \quad R^\psi(s) = \left(\frac{s}{L}\right)^0\left(1 - \frac{s}{L}\right)^1, \quad R^u(s) = \left(\frac{s}{L}\right)^0\left(1 - \frac{s}{L}\right)^1
$$

On the other hand, as it was mentioned earlier $T_i(s)$'s are an orthogonal set. In this paper, the Chebyshev polynomials orthonormal set which its elements can be defined through a recursive relation is adjusted (Ref. [37]):

$$
T_1(s) = 1, T_2(s) = 2\frac{s}{L} - 1, T_i(s) = 2\left(2\frac{s}{L} - 1\right)T_{i-1}(s) - T_{i-2}(s), \quad i = 2, 3, \ldots
\tag{27}
$$

The last step, with the intention of releasing the discretize nonlinear in time equations of motion is accomplished by the substitution of the separated displacement, i.e. Eq. (26), into the ensuing relation obtained from minimizing the action integral:

$$
\frac{\partial}{\partial A_i}\delta S = 0, \quad \frac{\partial}{\partial B_m}\delta S = 0, \text{and} \frac{\partial}{\partial C_r}\delta S = 0
\tag{28}
$$

The subsequent relations are reshuffled into a matrix from as:

$$
\{[\mathbf{M}]\}[\ddot{\mathbf{q}}] + \{[\mathbf{K}] - \omega_R^2[\mathbf{K}]^{\text{rotation}} - N_{ss}^T[\mathbf{K}]^{\text{thermal}}\}[\mathbf{q}] = \omega_R^2[\mathbf{F}]^{\text{rotation}} + N_{ss}^T[\mathbf{F}]^{\text{NT}} + M_{ss}^T[\mathbf{F}]^{\text{MT}} + R_{ss}^T[\mathbf{F}]^{\text{RT}}
\tag{29}
$$

where $[\mathbf{q}] = [\mathbf{A}, \mathbf{B}, \mathbf{C}]^T$ is the Ritz coefficients vector, and $\alpha[\mathbf{F}]^\beta$'s are the force vectors. Moreover, $[\mathbf{M}]$ is the mass matrix. Furthermore, $[\mathbf{K}] \equiv [\mathbf{K}]^{(1)} + [\mathbf{K}]^{(2)} + [\mathbf{K}]^{(3)}$ is the nonlinear stiffness matrix includes a linear, i.e. $[\mathbf{K}]^{(1)}$, a nonlinear second-order, i.e. $[\mathbf{K}]^{(2)}$, and a nonlinear third-order, i.e. $[\mathbf{K}]^{(3)}$, stiffness matrices.

2.5. The free vibration analysis prior to buckling

Prior to bucking incidence we deal with a nonlinear problem due to the geometrical nonlinearity arises from the presumption of the von-Karman relations. Indeed, the mutual relation of the centrifugal force which leads to a prestressed deformation and the von-Karman strain-displacement relation creates a geometrically nonlinear problem. Hence, an iterative solution procedure produces the prestressed configuration. The Newton-Raphson scheme (Ref. [34]) is employed to treat the nonlinear static displacements. From this perspective, at a specified temperature and rotating velocity we deal with the following nonlinear problem:

$$\{[\mathbf{K}]-\omega_R^2[\mathbf{K}]^{\text{rotation}}-N_{ss}^T[\mathbf{K}]^{\text{thermal}}\}[\mathbf{q}]=\omega_R^2[\mathbf{F}]^{\text{rotation}}+N_{ss}^T[\mathbf{F}]^{\text{NT}}+M_{ss}^T[\mathbf{F}]^{\text{MT}}+R_{ss}^T[\mathbf{F}]^{\text{RT}} \tag{30}$$

The following procedure delivers the natural frequencies for a rotating CNTRC beam:

1. At first the linearized prestressed equations of motion resulted by ignoring the nonlinear stiffness matrices from Eq. (30), i.e. $\{[\mathbf{K}]^{(1)}-\omega_R^2[\mathbf{K}]^{\text{rotation}}-N_{ss}^T[\mathbf{K}]^{\text{thermal}}\}[\mathbf{q}]=\omega_R^2[\mathbf{F}]^{\text{rotation}}+N_{ss}^T[\mathbf{F}]^{\text{NT}}+M_{ss}^T[\mathbf{F}]^{\text{MT}}+R_{ss}^T[\mathbf{F}]^{\text{RT}}$, is solved to release the Ritz coefficients. Subsequently, the first approximation of the prestressed configuration, i.e. $[\mathbf{q}]$, is achieved.
2. The latest Ritz coefficients are employed to create the nonlinear stiffness matrices. It is noteworthy that the existing nonlinear terms where for instance include $\frac{d^2}{dx^2}$ are determined by the use of the latest Ritz coefficients alongside with the second derivative of the first relation in Eq. (26). The tangent matrix, $[\mathbf{T}]=[\mathbf{K}]^{(1)}+2[\mathbf{K}]^{(2)}+3[\mathbf{K}]^{(3)}$ (Ref. [34]), is also created for the sake of determination of the evolution of the Ritz coefficients (Ref. [34]). If this evolution is beyond our desired precision the process is iterated in this step. After reaching the required accuracy we will go to the next step.
3. The eigen-value problem consists of the latest nonlinear stiffness and the mass matrices supplies natural frequencies and the corresponding eigen-modes.

2.6. The free vibration analysis after the buckling incidence

To examine the free vibrations of the rotating CNTRC beam after a probable buckling incidence in a series of certain cases of the boundary conditions, the solution procedure is different. The upcoming scheme brings us the fundamental natural frequency after the buckling incidence of a rotating CNTRC beam which its material properties depend on the temperature. We put the opening critical temperature equal to the reference temperature, i.e. 300 K.

1. At the newest critical temperature and a given rotational velocity the first two steps of the raised procedure in Sect. 2.5 is performed to deliver us the prestressed configuration.
2. Through the use of the prestressed configuration the elastic matrix $[\mathbf{K}]-\omega_R^2[\mathbf{K}]^{\text{rotation}}$ and the geometric matrix $[\mathbf{K}]^{\text{thermal}}$ are determined.
3. The eigen-problem consists of the elastic and the geometrical matrices release the critical thermal axial force resultant and the associated eigen-vector. Subsequently, the critical temperature change is accessible. By comparing the last two critical temperature changes, if the favorable accuracy is achieved the procedure is terminated. Otherwise, the process is resumed from the first step of the current itemized process.

Thereafter, the critical buckling temperature difference and the associated eigen-vector are employed as the initiating point for the free vibration examination after the buckling incidence. The material particle at the center of the area of the cross section located at the mid-span of the rotating CNTRC beam is picked as the observing point. The final desired transverse displacement for the observing point is assumed. The final desired deflection is divided into some pieces by assuming a step size. In our calculation to have smooth curves the step size has been considered as 0.1 *h*. Therefore, the first regarded transverse displacement for the observing point is 0.1 *h*.

1. The latest eigen-vector associated to the last critical temperature is scaled to create a transverse displacement at the observing point same as the latest regarded transverse displacement for the observing point.
2. Employing the scaled eigen-vector the nonlinear stiffness matrices are determined. Subsequently, the nonlinear elastic and tangent matrices are specified.
3. The nonlinear elastic and geometrical matrices are implemented to establish an eigen-problem that releases the updated critical temperatures along with the accompanying eigen-vector. If the appropriate accuracy for the critical temperature is obtained the regarded transverse displacement for the observing point is augmented by the assumed step size and the process is continued until reaching the maximum considered transverse displacement for the observing point. Otherwise, the procedure is resumed from step 1 of the current itemized process. It must be pointed out that for each regarded deflection for the observing point, the associated tangent matrix and the mass matrix are used to deliver the corresponding fundamental natural frequency.

3. Discussion and results

The exploration on the first natural frequency is addressed at this spot.

Table 2
The P_is constants employed for the determination of the stainless steel 304 and silicon nitride thermo-mechanical features (Ref. [31]).

Material	P	P_0	P_{-1}	P_1	P_2	P_3
$SUS304$	E[Pa]	201.04×10^9	0	3.079×10^{-4}	-6.534×10^{-7}	0
	$\alpha\ [\frac{1}{K}]$	12.33×10^{-6}	0	8.086×10^{-4}	0	0
	ν	0.28	0	0	0	0
	ρ [kg/m^3]	8166	0	0	0	0
Si_3N_4	E[Pa]	348.43×10^9	0	-3.07×10^{-4}	2.16×10^{-7}	-8.946×10^{-11}
	$\alpha\ [\frac{1}{K}]$	5.8723×10^{-6}	0	9.095×10^{-4}	0	0
	ν	0.28	0	0	0	0
	ρ [kg/m^3]	2170	0	0	0	0

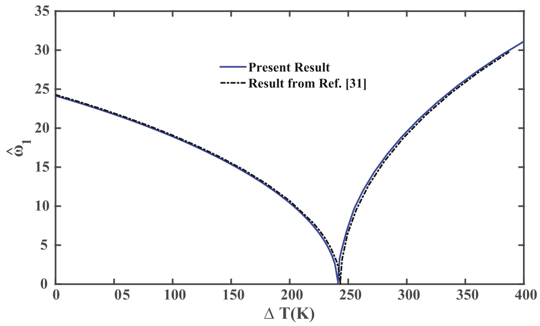

Fig. 2. The dimensionless fundamental natural frequency of a rotating three-layered clamped-clamped (CC) FG beam prior to and after the buckling incidence.

3.1. Verification of the results

First, the precision of the expanded formulation and the proposed solution scheme are verified. In this respect, the fundamental natural frequency of a rotating clamped-clamped (CC) symmetric three-layered FG Euler-Bernoulli beam is studied (Ref. [31]). The host layer is made of metal and specifically it is Stainless-Steel 304, $SUS304$. Two FG facesheets are attached to the bottom and the top surfaces of the host layer. They are graded linearly from a ceramic phase which is Silicon Nitride Si_3N_4 at the outer surface of the facesheets to the metal phase at the interface surface with the host layer which is $SUS304$. The thermo-mechanical material features, i. e. P, of the ceramic and the metal phases depend on the temperature according to $P = P_0(P_{-1}T^{-1} + 1 + P_1T^1 + P_2T^2 + P_3T^3)$ (Ref. [31]) wherein T is the current temperature in K and P_i's are the constants associated to a specific thermo-mechanical characteristic exposed in Table 2. The beam length to the total thickness ratio is $L/h = 30$, the host layer and the facesheets thicknesses to the total thickness proportions are, respectively, $\frac{h_c}{h} = 0.75$, $h_b = h_t = 0.125h$ and the hub radius is $R = 0.1L$. The current dimensionless fundamental natural frequency in comparison with the associated one from Ref. [31] is shown in Fig. 2 for $\widehat{\Omega} \equiv 100\omega_R L\sqrt{\frac{\rho_m}{E_m^{ref}}} = 10$ where E_m^{ref} is the elasticity modulus of the metal phase at the reference temperature. It is observed that before the buckling incidence the current fundamental natural frequency is lower than the one predicted by the Euler-Bernoulli assumption. Moreover, the current critical temperature which leads to the instability of the rotating beam in regard to the RSDT is smaller than the one reported in Ref. [31] in the context of Euler-Bernoulli presumption.

The other instance is a rotating CF CNTRC beam modeled in accordance with the Timoshenko beam theory (Ref. [28]). The beam rotates at $\omega_R = 10000$ rpm. The beam height is $h = 0.01$ m. The length to the height of the beam and the hub radius are, respectively, 100, and $0.1L$. The host beam is made of epoxy and its thermo-mechanical properties are $E^m = (3.52 - 0.0034T)$ GPa, $\rho^m = 1150$ kg/m^3, $\nu^m = 0.34$, $G^m = \frac{E^m}{2(1+\nu^m)}$ and $\alpha^m = 45 \times 10^{-6}(1 + 0.0005\Delta T)$ 1/K. The matrix is reinforced by CNT which is an (10, 10) armchair single-walled CNT (SWCNT). The thermo-mechanical attributes depend on the temperature according to a polynomial function (Ref. [33]):

$$P = P_0 + P_1\left(\frac{T}{T_0}\right) + P_2\left(\frac{T}{T_0}\right)^2 + P_3\left(\frac{T}{T_0}\right)^3 + P_4\left(\frac{T}{T_0}\right)^4 \tag{31}$$

where T is the current temperature. It is worth to note that P can be elastic modulus, shear modulus, the Poisson' ratio, the mass density, and the thermal expansion constant. For any specific mentioned characteristics P_i's are defined in Table 3. The achieved outcomes for the first three natural frequencies and for three different CNT dispersion patterns at 300 K are presented in Table ?? By a glance at the outcomes the validity of the present results is acknowledged.

Table 3
The P_is constants employed in Eq. (31) for the determination of the CNT thermo-mechanical features (Ref. [33]).

P	P_0	P_1	P_2	P_3	P_4
E_{11}[TPa]	6.56537	−1.76156	1.13347	−0.32260	0.03193
E_{22}[TPa]	8.22710	−2.19725	1.41176	−0.40125	0.03964
G_{12}[TPa]	1.10442	1.88427	−1.47623	0.49029	−0.05829
$\alpha_{11}[10^{-6}\frac{1}{K}]$	−1.12800	6.88290	−2.60621	0.31023	−0.00054
$\alpha_{22}[10^{-6}\frac{1}{K}]$	5.435933	−0.29201	0.02268	0.00182	−0.00023
ν_{12}	0.17500	0	0	0	0
ρ [kg/m^3]	1400	0	0	0	0

Table 4
The number of the required terms in Ritz technique for the convergence of the post-critical dimensionless natural frequency of a rotating clamped-simply (CS) FGX CNTRC beam at 220 K.

Number of Ritz Terms	ω_1^*
$N = 5$	24.2
$N = 7$	24.4
$N = 9$	24.5
$N = 11$	24.5

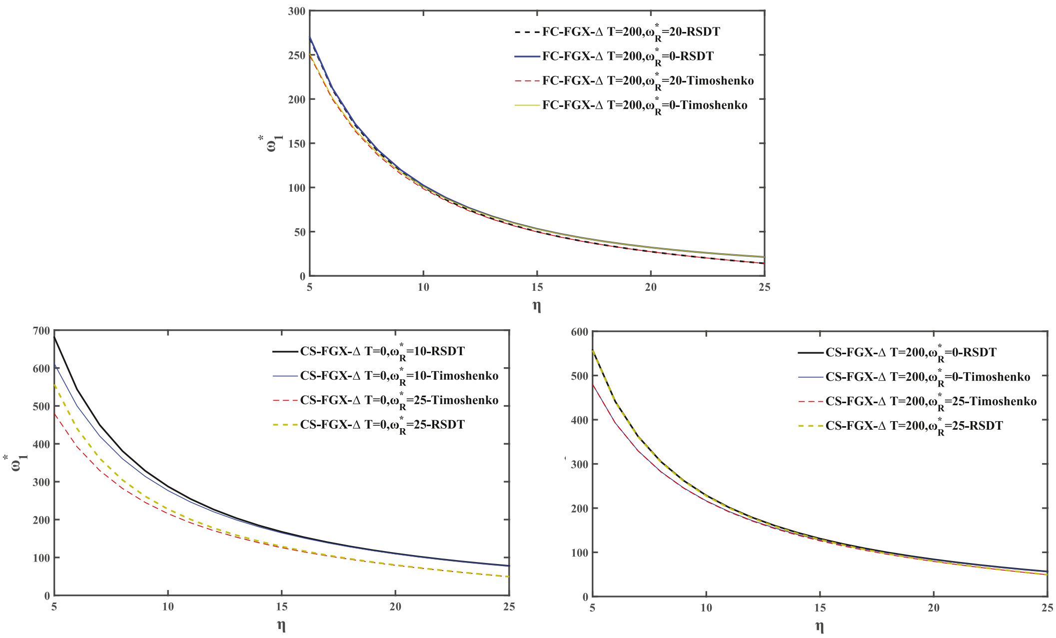

Fig. 3. The dimensionless first natural frequency relating to the length to the height of the beam for a rotating FGX CNTRC beam in the context of the RSDT and Timoshenko beam theory for two different boundary condition types.

A parametric study is established in this part to find out how the free vibration outcomes of a rotating CNTRC beams are impressed by the geometrical, and the mechanical features and loading conditions. In this respect, all the thermo-mechanical features of the CNT are the same as addressed in Ref. [33] exposed in Table 3. Moreover, the matrix is epoxy with $E^m = (3.52 - 0.0034T)$ GPa, $\rho^m = 1150$ kg/m^3, $\nu^m = 0.34$, $G^m = \frac{E^m}{2(1+\nu^m)}$ and $\alpha^m = 45 \times 10^{-6}(1 + 0.0005\Delta T)$ 1/K (Ref. [33]). The length to the height of the beam, and the hub radius, are, $\frac{L^{ref}}{h^{ref}} = 40$, and $R^{ref} = 0.1L^{ref}$, in order. The dimensionless rotation speed and the fundamental natural frequency are defined, respectively, by $\omega_R^* = \omega_R\tau$, and $\omega_1^* = \omega_1\tau$ wherein ω_1 is the dimensional fundamental natural frequency and $\tau \equiv \frac{L^2}{h}\sqrt{\frac{\rho_m}{E_m^{ref}}}$ is the characteristic time.

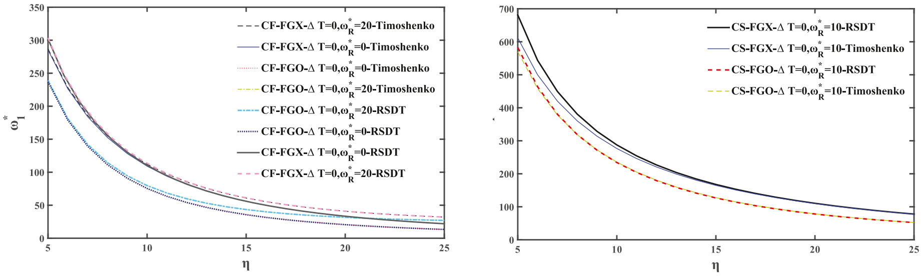

Fig. 4. The dimensionless first natural frequency relating to the length to the height of the beam for a rotating FGX/FGO CNTRC beam in the context of the RSDT and Timoshenko beam theory for two different boundary condition types.

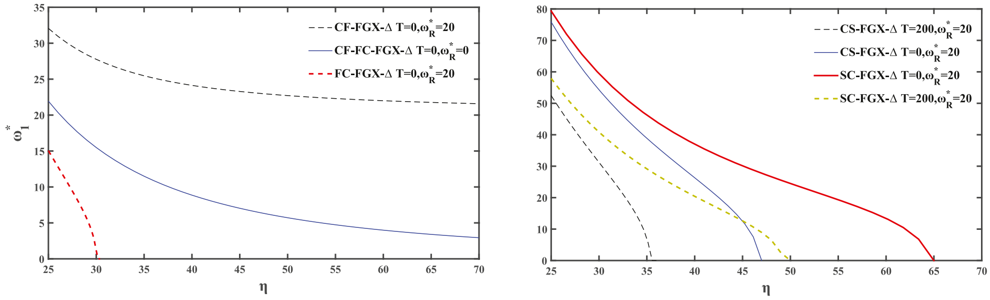

Fig. 5. The dimensionless first natural frequency relating to the length to the height of the beam for a rotating FGX CNTRC beam with four different boundary condition types.

Initially we establish a convergence examination to find out how many terms, i.e. N, are required in the Ritz technique for the sake of presenting precise results. The results of post-critical dimensionless natural frequency for a rotating clamped-simply (CS) FGX CNTRC beam at 220 K are exposed in Table 4 for $\omega_R^* = 15$. It is inferred that a good precision can be observed by $N = 9$.

In Fig. 3 the impact of the employed shear deformation theory in terms of the length to the height of the beam on the determination of the dimensionless first natural frequency of the rotating FC, and CS FGX CNTRC beams is examined for two different temperatures. It is deduced that for a rotating CS FGX beam the effect of the shear deformation theory type is more distinguishable with respect to a rotating FC FGX beam. Moreover, the increment of the temperature increases the influence of the employed shear deformation theory on the outcomes. This conclusion is owing to the fact that as a result of the increment of the temperature the beam stiffness reduces and subsequently the beam deals with more bending rotation in its cross sections. Subsequently, the type of the employed shear deformation theory becomes more determinative. For a rotating CS FGX beam, by the increment of the length to the height of the beam, approximately after 12, the predictions in the framework of the both shear deformation theories coincide to each other while for a FC rotating FGX beam the threshold value is about 10. Furthermore, by the increment of the temperature the impact of rotational velocity on the first natural frequency reduces. Moreover, by the increment of the length to the height of the beam the effect of the rotation speed is more distinguishable. The implication is that when the slenderness ratio increases the beam gets softer. Subsequently, the rotational velocity deflects the beam more readily.

The importance of the type of the shear deformation theory on the prediction of the dimensionless fundamental natural frequency is depicted in Fig. 4 for a rotating CF FGX/FGO CNTRC beam and a rotating CS FGX/FGO CNTRC beam. Is is deduced that the fundamental natural frequency of a rotating FGO CNTRC beam is less affected by the shear deformation theory type. In other words, the first natural frequency of a rotating FGO CNTRC beam is approximately invariant with respect the employed shear deformation theory. According to these two recent studies it is inferred that the type of the employed shear deformation theory is more crucial for rotating CS FGX beams with slenderness ratios below 12.

The length to the height of the beam influence on the dimensionless fundamental natural frequency of a rotating FC/CF and a rotating simply-clamped(SC)/CS FGX beam is depicted in Fig. 5. It is implicated that although the corresponding results for the stationary CF and FC FGX beams are the same however, they are qualitatively and quantitatively different when the beam starts to rotate; a rotating FC beam may become unstable due to the buckling incidence while a rotating CF beam never lose its stability because of the buckling incidence. On the other hand, the fundamental natural frequency of a rotating CS beam also differs quantitatively from the one for a rotating SC beam. Moreover, the increasing of the temperature reduces the first natural frequency as well as the critical value for the length to the height of the beam of the rotating SC/CS beams. Furthermore, the stiffness of a rotating CS beam is always less than the one for a rotating SC beam in the same conditions.

After a comprehensive examination on the first natural frequency of the rotating CNTRC beams in thermal ambient, henceforth, the

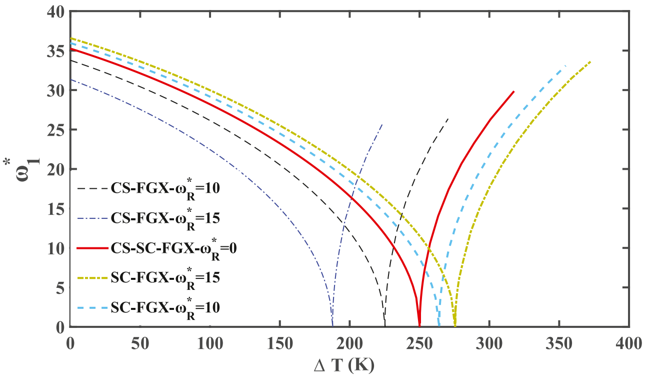

Fig. 6. The dimensionless first natural frequency for a rotating FGX CNTRC beam prior to and after the buckling incidence for two different supports.

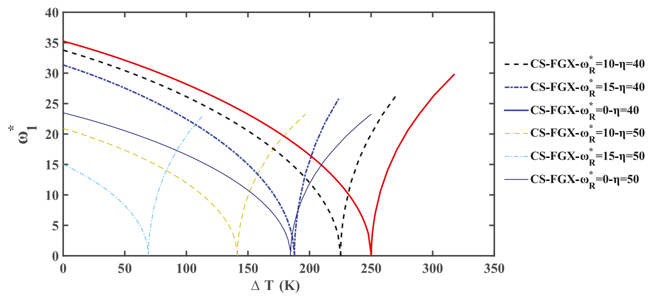

Fig. 7. The influence of the length to the height of the beam on the dimensionless first natural frequency of a rotating CS FGX CNTRC beam prior to and after the buckling incidence.

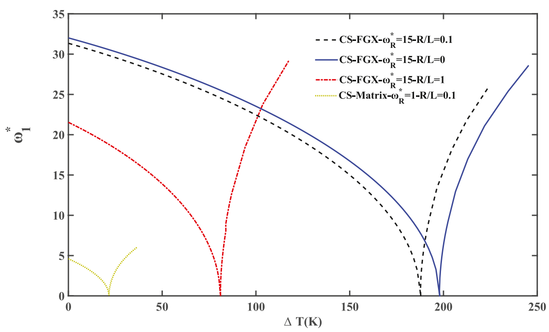

Fig. 8. The influence of the hub radius on the dimensionless first natural frequency of a rotating CS FGX CNTRC beam prior to and after the buckling incidence.

free vibrations of the rotating beams prior to and after the buckling incidence for the rotating CS/SC CNTRC beams are examined. The effect of the support and the rotation speed on the first natural frequency is captured in Fig. 6. In agreement with the implication achieved in the free vibrations outcomes prior to buckling incidence, the stationary CS and SC beams behave similarly before and after the buckling occurrence. Nonetheless, the increment of the rotating velocity shifts the response of the rotating CS beam to the left more and more while the one for the rotating SC beam transfers to the right. It is deduced that the increase of the rotating velocity alleviates the stiffness of the CS beam while intensifies the stiffness of the SC beam. Moreover, after the buckling incidence the growth of the rotating velocity enhances the first natural frequency of a rotating CS beam at the same temperature while a reverse trend is predicted before the buckling occurrence for the rotating CS beam. An opposite tendency is determined for a rotating SC beam.

The dimensionless first natural frequency for a rotating CS FGX CNTRC beam for two different slenderness ratios and different rotation speeds is shown in Fig. 7. It is deduced that the first natural frequency is more impressed by the rotation speed variation at larger slenderness ratios. This is due to the fact that the increment of the length to the height of the beam is associated with a reduction in the stiffness of the beam. Subsequently, the rotation speed can affect more the fundamental natural frequency at higher slenderness ratios.

The hub radius variation consequence on the dimensionless first natural frequency of a rotating CS FGX CNTRC beam is depicted in Fig. 8 in comparison with the one for a rotating CS beam composed of just matrix phase. It is seen that the stiffness of the rotating beam decreases by the increment of the hub radius. Moreover, the first natural frequency prior to the instability incidence is less affected by the variation in the ratio at the same temperature in comparison with the corresponding value after the buckling occurrence. Moreover, it is seen that how the CNT reinforcement can improve the buckling instability temperature as well as the fundamental natural frequency. The implication is as a consequence of improving the stiffness of the rotating beam by adjoining the CNT phase.

4. Conclusions

For the first time, the fundamental natural frequency of rotating CNTRC beams prior to the thermal buckling incidence accompanied by the associated one after the buckling incidence was analyzed, in this paper. The weak form of the motion equations was obtained in the context of the third-order shear deformation theory of Reddy (RSDT). The beam was considered to be in a thermal ambient deals with a constant temperature rising across its height. The Ritz technique was employed with the aim of discretizing the weak form of the motion equations in space. By developing an efficient solution the first natural frequency of rotating CNTRC beams prior to and after a possible buckling incidence for the supports conditions which induce the feasibility of such instability to a rotating beam was studied. The conditions that enforce us to implement the RSDT were justified. Moreover, the support type impact on the first natural frequency of the rotating CNTRC beams was studied to highlight the disagreements between the rotating and stationary CNTRC beams. The findings are as follows;

- The outcomes based upon the RSDT deviate from the results in the framework of the Timoshenko beam theory approximately below the length to the height of the beam equal to 12 for CS FGX CNTRC beams. However, for the FGO CNTRC beams the results in reference to the both mentioned theories approximately coincide to each other.
- The length to the height of the beam threshold value at which the results of the third- and first-order shear deformation theories concur depends on the boundary condition type and also the CNT dispersion pattern type.
- For stationary beams in thermal ambient there is no difference between a clamped-free and a free-clamped beam as well as a clamped-simply and a simply-clamped beam. However, for rotating beams qualitative and quantitative differences are observed.
- Although by the growth of the rotational velocity at a specified temperature the first natural frequency of a rotating CS CNTRC beam reduces prior to the buckling incidence, after the buckling occurrence a reverse behavior is detected. It is worth to note that the SC CNTRC beam treats adversely.

Sample CRediT author statement

Xinli Xu: Conceptualization, Methodology, Software, Validation, Formal analysis **Chunwei Zhang:** Conceptualization, Methodology, Software, Data Curation, Writing - Review & Editing, Visualization, Project administration **Afrasyab Khan:** Conceptualization, Data Curation, Writing - Review & Editing, Visualization, Supervision, Project administration **Tamer A. Sebaey:** Conceptualization, Validation, Data Curation, Writing - Review & Editing, Visualization, Supervision, Project administration **Mohammad Alkhedher:** Investigation, Resources, Data Curation, Writing - Original Draft, Visualization, Supervision, Project administration.

Declaration of competing interest

The authors declare that they have no known competing financial interests or personal relationships that could have appeared to influence the work reported in this paper.

Acknowledgement

This research is financially supported by the Ministry of Science and Technology of China (Grant No. 2019YFE0112400; 2017YFC0703603), the Taishan Scholar Priority Discipline Talent Group program funded by the Shan Dong Province, and the first-class discipline project funded by the Education Department of Shandong Province.

Appendix I

The thermal stress and higher order stress resultants:

$$\{N_{ss}^T, M_{ss}^T, R_{ss}^T\} = \int_{-\frac{1}{2}h}^{\frac{1}{2}h} [Q_{11}(z)\alpha_{11}(z)\{1, z, z^3\}]\mathrm{d}z \tag{32}$$

The elastic stiffnesses:

$$\{A_{ii}, B_{ii}, D_{ii}, C_{ii}, F_{ii}, G_{ii}\} = \int_{-\frac{1}{2}h}^{\frac{1}{2}h} [Q_{ii}(z)\{1, z, z^2, z^3, z^4, z^6\}]\mathrm{d}z \tag{33}$$

The inertial terms:

$$\{I_i\} = \int_{-\frac{1}{2}h}^{\frac{1}{2}h} [\rho(z)\{z^i\}]\mathrm{d}z \tag{34}$$

References

[1] J.N. Reddy, Mechanics of Laminated Composite Plates and Shells: Theory and Analysis, CRC press, 2003.
[2] P. Zhu, Z.X. Lei, K.M. Liew, Static and free vibration analyses of carbon nanotube-reinforced composite plates using finite element method with first order shear deformation plate theory, Compos. Struct. 94 (4) (2012) 1450–1460.
[3] H.S. Shen, Y. Xiang, Nonlinear analysis of nanotube-reinforced composite beams resting on elastic foundations in thermal environments, Eng. Struct. 56 (2013) 698–708.
[4] F. Lin, Y. Xiang, Vibration of carbon nanotube reinforced composite beams based on the first and third order beam theories, Appl. Math. Model. 38 (15–16) (2014) 3741–3754.
[5] B.A. Selim, L.W. Zhang, K.M. Liew, Vibration analysis of CNT reinforced functionally graded composite plates in a thermal environment based on Reddy's higher-order shear deformation theory, Compos. Struct. 156 (2016) 276–290.
[6] B. Safaei, P. Naseradinmousavi, A. Rahmani, Development of an accurate molecular mechanics model for buckling behavior of multi-walled carbon nanotubes under axial compression, J. Mol. Graph. Model. 65 (2016) 43–60.
[7] S.S. Mirjavadi, A. Matin, N. Shafiei, S. Rabby, B. Mohasel Afshari, Thermal buckling behavior of two-dimensional imperfect functionally graded microscale-tapered porous beam, J. Therm. Stresses 40 (10) (2017) 1201–1214.
[8] S. Sahmani, M.M. Aghdam, Axial postbuckling analysis of multilayer functionally graded composite nanoplates reinforced with GPLs based on nonlocal strain gradient theory, Eur. Phys. J. Plus 132 (11) (2017) 1–17.
[9] S.S. Mirjavadi, S. Rabby, N. Shafiei, B.M. Afshari, M. Kazemi, On size-dependent free vibration and thermal buckling of axially functionally graded nanobeams in thermal environment, Appl. Phys. A 123 (5) (2017) 315.
[10] H.S. Shen, Y. Xiang, F. Lin, D. Hui, Buckling and postbuckling of functionally graded graphene-reinforced composite laminated plates in thermal environments, Compos. B Eng. 119 (2017) 67–78.
[11] J. Yang, D. Chen, S. Kitipornchai, Buckling and free vibration analyses of functionally graded graphene reinforced porous nanocomposite plates based on Chebyshev-Ritz method, Compos. Struct. 193 (2018) 281–294.
[12] S.S. Mirjavadi, B. Mohasel Afshari, N. Shafiei, S. Rabby, M. Kazemi, Effect of temperature and porosity on the vibration behavior of two-dimensional functionally graded micro-scale Timoshenko beam, J. Vib. Contr. 24 (18) (2018) 4211–4225.
[13] H.G. Lin, D.Q. Cao, Y.Q. Xu, Vibration, buckling and aeroelastic analyses of functionally graded multilayer graphene-nanoplatelets-reinforced composite plates embedded in piezoelectric layers, Int. J. Appl. Mech. 10 (2018) 1850023, 03.
[14] A.A. Hamzah, H.K. Jobair, O.I. Abdullah, E.T. Hashim, L.A. Sabri, An investigation of dynamic behavior of the cylindrical shells under thermal effect, Case Stud. Therm. Eng. 12 (2018) 537–545.
[15] A. Eyvazian, S.A. Taghizadeh, A.M. Hamouda, F. Tarlochan, M. Moeinifard, M. Gobbi, Buckling and crushing behavior of foam-core hybrid composite sandwich columns under quasi-static edgewise compression, J. Sandw. Struct. Mater. (2019), https://doi.org/10.1177/1099636219894665, 1099636219894665.
[16] J.J. Mao, W. Zhang, Buckling and post-buckling analyses of functionally graded graphene reinforced piezoelectric plate subjected to electric potential and axial forces, Compos. Struct. 216 (2019) 392–405.
[17] A.M. Fattahi, B. Safaei, N.A. Ahmed, A comparison for the non-classical plate model based on axial buckling of single-layered graphene sheets, Eur. Phys. J. Plus 134 (11) (2019) 555.
[18] A. Eyvazian, A.M. Hamouda, F. Tarlochan, S. Mohsenizadeh, A.A. Dastjerdi, Damping and vibration response of viscoelastic smart sandwich plate reinforced with non-uniform Graphene platelet with magnetorheological fluid core, Steel Compos. Struct. 33 (6) (2019) 891–906.
[19] J. Zhao, K. Choe, C. Shuai, A. Wang, Q. Wang, Free vibration analysis of functionally graded carbon nanotube reinforced composite truncated conical panels with general boundary conditions, Compos. B Eng. 160 (2019) 225–240.
[20] B. Safaei, The effect of embedding a porous core on the free vibration behavior of laminated composite plates, Steel Compos. Struct. 35 (5) (2020) 659–670.
[21] A. Eyvazian, D. Shahsavari, B. Karami, On the dynamic of graphene reinforced nanocomposite cylindrical shells subjected to a moving harmonic load, Int. J. Eng. Sci. 154 (2020) 103339.
[22] X. Zhao, W.D. Zhu, Y.H. Li, Analytical solutions of nonlocal coupled thermoelastic forced vibrations of micro-/nano-beams by means of Green's functions, J. Sound Vib. 481 (2020) 115407.
[23] J. Zheng, C. Zhang, F. Musharavati, A. Khan, T.A. Sebaey, Thermo-mechanical buckling analysis of FG-GNPs reinforced composites sandwich microplates using a trigonometric four-variable shear deformation theory, Case Stud. Therm. Eng. (2021) 101120.
[24] T.T. Tran, P.C. Nguyen, Q.H. Pham, Vibration analysis of FGM plates in thermal environment resting on elastic foundation using ES-MITC3 element and prediction of ANN, Case Stud. Therm. Eng. 24 (2021) 100852.
[25] J. Li, G. Wang, S. Liu, J. Lin, Y. Guan, G. Zhao, T. Wu, Efficient thermomechanical analysis of functionally graded structures using the symmetric SPH method, Case Stud. Therm. Eng. 25 (2021) 100889.
[26] A.M. Fattahi, B. Safaei, Z. Qin, F. Chu, Experimental studies on elastic properties of high density polyethylene-multi walled carbon nanotube nanocomposites, Steel Compos. Struct. 38 (2) (2021) 177–187.
[27] H. Arvin, On parametrically excited vibration and stability of beams with varying rotating speed, Iran. J. Sci. Technol. Trans. Mech. Eng. 43 (2) (2019) 177–185.
[28] M. Heidari, H. Arvin, Nonlinear free vibration analysis of functionally graded rotating composite Timoshenko beams reinforced by carbon nanotubes, J. Vib. Contr. 25 (14) (2019) 2063–2078.
[29] S. Khosravi, H. Arvin, Y. Kiani, Vibration analysis of rotating composite beams reinforced with carbon nanotubes in thermal environment, Int. J. Mech. Sci. 164 (2019) 105187.
[30] S.M.H. Hosseini, H. Arvin, Free vibration analysis of pre/post-buckled rotating functionally graded sandwich micro-beams, Microsyst. Technol. (2020) 1–13, https://doi.org/10.1007/s00542-020-04986-4.
[31] H. Arvin, S.M.H. Hosseini, Y. Kiani, Free vibration analysis of pre/post buckled rotating functionally graded beams subjected to uniform temperature rise, Thin-Walled Struct. 158 (2021) 107187.
[32] H.S. Shen, Nonlinear bending of functionally graded carbon nanotube-reinforced composite plates in thermal environments, Compos. Struct. 91 (1) (2009) 9–19.

[33] S. Khosravi, H. Arvin, Y. Kiani, Interactive thermal and inertial buckling of rotating temperature-dependent FG-CNT reinforced composite beams, Compos. B Eng. 175 (2019) 107178.
[34] J.N. Reddy, An Introduction to Nonlinear Finite Element Analysis Second Edition: with Applications to Heat Transfer, Fluid Mechanics, and Solid Mechanics, OUP, Oxford, 2014.
[35] L. Meirovitch, Principles and Techniques of Vibrations, vol. 1, Prentice Hall, Upper Saddle River, NJ, 1997.
[36] Y. Kiani, Free vibration of functionally graded carbon nanotube reinforced composite plates integrated with piezoelectric layers, Comput. Math. Appl. 72 (9) (2016) 2433–2449.
[37] J.C. Mason, D.C. Handscomb, Chebyshev Polynomials, CRC press, 2002.